

Combined micro–macro integration scheme from an invariance principle: application to ferrofluid dynamics

Patrick Ilg^{a,1}

^a*Inst. Theoret. Physik, TU Berlin, Sekr. PN 7-1, Hardenbergstr. 36, D-10623
Berlin, Germany*

Iliya V. Karlin^{b,c}

^b*Department of Materials, Institute of Polymers, ML J19, ETH Zürich, CH-8092
Zürich, Switzerland*

^c*Institute of Computational Modelling SB RAS, 660036 Krasnoyarsk, Russia*

Abstract

A method for the combination of microscopic and macroscopic simulations is developed which is based on the invariance of the macroscopic relative to the microscopic dynamics. The method recognizes the onset and breakdown of the macroscopic description during the integration. We apply this method to the case of ferrofluid dynamics, where it switches between direct Brownian dynamics simulations and integration of the constitutive equation.

Key words: Multiscale simulation, Reduced description, Constitutive equation, Kinetic theory, Magnetic liquids

PACS: 05.10.-a Computational methods in statistical physics and nonlinear dynamics, 83.10.Gr Constitutive relations, 05.20.Dd Kinetic theory, 75.50.Mm Magnetic liquids

1 Introduction

The understanding of the macroscopic dynamics from the underlying microscopic time evolution is a central issue of non-equilibrium statistical mechanics. The massive use of computer simulations over the last years has led to new approaches to this very old problem. Among others, we mention Legendre integrators [1,2,3], the CONFESSIT method [4], adaptive mesh refinement and multiscale modeling [5,6]. The last two methods do not require knowledge of the macroscopic equations. On the other hand, there has been much effort to derive approximate macroscopic equations from the microscopic dynamics, which yield reliable results under various circumstances (see e.g. Ref. [7] for an overview of constitutive equations for polymer liquids). Here, we follow the approach proposed in Ref. [8] to combine microscopic and macroscopic simulations in a combined integration scheme which recognizes the onset and breakdown of the chosen macroscopic description during the simulation. Note, that the breakdown of a chosen macroscopic description does not imply a similar breakdown of other, improved macroscopic descriptions. Instead of improving the macroscopic equations, which is the aim of many works on closure approximations (see e.g. [1,2] and references therein), we here keep the chosen macroscopic description and use it as long and as frequently in the simulation as possible. While this integration scheme was used in Ref. [8] to detect the onset of the macroscopic description, we here present the full scheme that switches back and forth between microscopic and macroscopic simulations. We apply this scheme to well-known models of ferrofluid dynamics where it decides between direct Brownian dynamics simulations and integration of the constitutive equation.

2 Invariance principle and combined integration scheme

In order to keep the paper self-contained, we briefly summarize the main ideas of the combined integration scheme based on the invariance principle proposed in Refs. [8,9]. We assume a given microscopic description of the system, where the microscopic variables are denoted by f . The microscopic dynamics is specified by the vector field J ,

$$\frac{\partial}{\partial t}f = J(f). \tag{1}$$

Email addresses: ilg@itp.physik.tu-berlin.de (Patrick Ilg),
ikarlin@mat.ethz.ch (Iliya V. Karlin).

¹ corresponding author; phone: +49-30 314 25225; fax: +49-30 314 21130

In addition, we assume that the set of macroscopic variables \mathbf{M} has been chosen. Typically, $f(x)$ is the distribution function over the set of microscopic coordinates x and \mathbf{M} contains low-order moments of f . In this case, the macroscopic variables are linear functionals of the microscopic distribution function, $\mathbf{M} = \int dx \mathbf{m}(x)f(x)$. Although the method can be applied to more general situations, we here limit ourselves to this case for the sake of clarity.

The reduced or macroscopic description assumes not only closed-form macroscopic equations $\dot{\mathbf{M}}(\mathbf{M})$, but also a family of canonical distribution functions $f_{\mathbf{M}}(x)$ [1,2]. The canonical distribution functions satisfy the consistency relation $\mathbf{M} = \int dx \mathbf{m}(x)f_{\mathbf{M}}(x)$. Then, the macroscopic dynamics is given by

$$\dot{\mathbf{M}}(\mathbf{M}) = \int dx \mathbf{m}(x)J(f_{\mathbf{M}}(x)) \quad (2)$$

Different routes to the construction of $f_{\mathbf{M}}$ have been proposed. In many applications, the dynamic system Eq. (1) is equipped with a Lyapunov function S (the entropy, free energy, etc.), and the canonical distribution functions $f_{\mathbf{M}}$ are conditional maximizers of S subject to fixed \mathbf{M} [8].

In order to estimate the accuracy of the macroscopic description we define the defect of invariance $\Delta_{\mathbf{M}}(x)$ as the difference of the microscopic and macroscopic time derivative,

$$\Delta_{\mathbf{M}}(x) = J(f_{\mathbf{M}}) - \frac{\partial f_{\mathbf{M}}}{\partial \mathbf{M}} \cdot \dot{\mathbf{M}}(\mathbf{M}). \quad (3)$$

By construction, $\int dx \mathbf{m}(x)\Delta_{\mathbf{M}}(x) = 0$. If the defect of invariance $\Delta_{\mathbf{M}}(x)$ vanishes for all admissible values of \mathbf{M} , then the reduced description is called invariant and the family $f_{\mathbf{M}}$ represents the invariant manifold in the space of the microscopic variables. The invariant manifold is relevant if it is stable. Exact invariant manifolds are known only in very few cases. Corrections to the manifold $f_{\mathbf{M}}$ through minimizing $\Delta_{\mathbf{M}}$ is part of the so-called method of invariant manifolds [10,11].

Here, we exploit the invariance principle in a different way. Let $f(x; t|t_0)$ denote the microscopic variables at time t for given initial conditions at time $t_0 < t$. The values of the macroscopic variables at time t are given by $\mathbf{M}(t|t_0) = \int dx \mathbf{m}(x)f(x; t|t_0)$. On the other hand, the solution of the macroscopic equations (2) with corresponding initial conditions gives $\mathbf{M}^*(t|t_0)$. We denote with $\|\Delta\|$ the value of the defect of invariance (3) with respect to some norm $\|\bullet\|$ and $\epsilon > 0$ a fixed threshold value. If at time t the defect of invariance satisfies

$$\|\Delta_{\mathbf{M}(t|t_0)}\| < \epsilon, \quad (4)$$

it is said that the macroscopic description *sets on*, since the reduced description is sufficiently accurate. However, if

$$\|\Delta_{\mathbf{M}^*(t|t_0)}\| > \epsilon, \quad (5)$$

the macroscopic description *breaks down* since the accuracy of the macroscopic dynamics is insufficient. Therefore, the evaluation of the defect of invariance (3) on the current solution either to the macroscopic or to the microscopic dynamics and checking Eqs. (4) and (5) we can decide whether integration of the macroscopic dynamics is sufficiently accurate or not.

This information is used in the combined integration scheme to switch between microscopic and macroscopic simulations. The scheme is sketched in Fig. 1. Suppose at time t_0 the microscopic dynamics is integrated for given initial condition. The integration is continued until at time t_1 the inequality (4) is satisfied. At this point, the macroscopic dynamics is started with the actual values of the macroscopic variables, $\mathbf{M}^*(t_1) = \mathbf{M}(t_1|t_0)$. The macroscopic dynamics is integrated until the macroscopic description breaks down at a later time t_2 , which is signaled by $\|\Delta_{\mathbf{M}^*(t_2|t_1)}\| > \epsilon$. At this time it is necessary to switch back from the macroscopic to the microscopic simulations in order to achieve the required accuracy. The initial condition for the microscopic simulation at time t_2 is obtained from the macroscopic description, $f(x, t_2) = f_{\mathbf{M}(t_2)}(x)$. Then, the microscopic dynamics is integrated until the macroscopic description sets on etc. In the sequel, we demonstrate this scheme for the case of ferrofluid dynamics.

3 Kinetic models of ferrofluid dynamics

Ferrofluids are stable suspensions of nano-sized ferromagnetic colloidal particles in a suitable carrier liquid [12]. These fluids attract considerable interest due to their peculiar behavior, such as the magnetoviscous effect, the dependence of the viscosity coefficients on the magnetic field [13].

We here consider the kinetic model of ferrofluid dynamics proposed in Refs. [14,15]. In this model, the ferromagnetic particles are assumed to be identical, magnetically hard ferromagnetic monodomain particles. It is further assumed that the particles are of an ellipsoidal shape with axes ratio r and that the magnetic moment μ is oriented parallel to the symmetry axes of the particle. Let $f(\mathbf{u})$ denote the orientational distribution function to find a ferromagnetic particle with the orientation \mathbf{u} , where \mathbf{u} is a vector on the three-dimensional unit sphere. In the general notation of Sec. 2, the microscopic coordinates x are the orientations \mathbf{u} and $f(x)$ is the orientational distribution function $f(\mathbf{u})$. The

normalized macroscopic magnetization \mathbf{M} is given by $\mathbf{M} = \int d^2u \mathbf{u} f(\mathbf{u})$, where $\int d^2u$ denotes integration over the three-dimensional unit sphere. The normalization is performed with the saturation magnetization $M_{\text{sat}} = n\mu$, where n denotes the number density. In the presence of a local magnetic field \mathbf{H} and a velocity field \mathbf{v} , the dynamics is given by [12,16]

$$\frac{\partial}{\partial t} f = -\mathcal{L} \cdot \{(\boldsymbol{\Omega} \times \mathbf{u} + B\mathbf{u} \times \mathbf{D} \cdot \mathbf{u} - D_r \mathbf{h} \times \mathbf{u})f\} + D_r \mathcal{L} \cdot \mathcal{L} f \quad (6)$$

In Eq. (6) we have introduced the rotational operator $\mathcal{L} = \mathbf{u} \times \partial/\partial\mathbf{u}$, the vorticity $\boldsymbol{\Omega} = \nabla \times \mathbf{v}/2$, the symmetric velocity gradient $2\mathbf{D} = \nabla\mathbf{v} + (\nabla\mathbf{v})^T$, and the so-called shape factor $B = (r^2 - 1)/(r^2 + 1)$. The rotational diffusion coefficient D_r defines the rotational relaxation time $\tau = (2D_r)^{-1}$. The dimensionless magnetic field is defined by $\mathbf{h} = \mu\mathbf{H}/k_B T$, where k_B and T denote Boltzmann's constant and temperature, respectively. The equilibrium distribution

$$f_{\mathbf{h}}(\mathbf{u}) = \frac{h}{4\pi \sinh(h)} \exp[\mathbf{h} \cdot \mathbf{u}] \quad (7)$$

is the stationary solution to the kinetic equation (6) in the absence of flow. From Eq. (7), the equilibrium magnetization \mathbf{M}^{eq} is found to be given by $\mathbf{M}^{\text{eq}}/M_{\text{sat}} = L_1(h)\mathbf{h}/h$, where $h = \sqrt{\mathbf{h} \cdot \mathbf{h}}$ is the Langevin parameter and $L_1(x) = \coth(x) - x^{-1}$ denotes the Langevin function.

Except for special cases, exact solutions to the kinetic equation (6) are unknown and closed form equations for the magnetization cannot be derived exactly from Eq. (6). In order to solve the closure problem, the authors of Ref. [17] have suggested to use the family of equilibrium distributions (7), where the magnetic field \mathbf{h} is replaced by an effective field $\boldsymbol{\xi}$. Thus, the non-equilibrium magnetization is given by $\mathbf{M}/M_{\text{sat}} = L_1(\boldsymbol{\xi})\mathbf{n}$, where we have introduced the norm ξ of the effective field $\boldsymbol{\xi}$ and $\mathbf{n} = \boldsymbol{\xi}/\xi$. This so-called Effective Field Approximation (EFA) is a particular instance of the quasi-equilibrium or maximum entropy approximation. It is derived from extremizing the entropy functional $S[f] = -\int d^2u f(\mathbf{u}) \ln[f(\mathbf{u})/f_{\mathbf{h}}(\mathbf{u})]$ subject to the constraints of fixed normalization and fixed values of magnetization \mathbf{M} . Therefore, the set of macroscopic variables contains only the magnetization \mathbf{M} in the present case. For more details on the use of quasi-equilibrium approximation in the context of complex fluids see e.g. [1,2,3]. The macroscopic equation (2) becomes the magnetization equation

$$\dot{\mathbf{M}} = \boldsymbol{\Omega} \times \mathbf{M} + B \left[\left(1 - \frac{2L_2(\xi)}{\xi L_1(\xi)} \right) \mathbf{D} \cdot \mathbf{M} - \frac{L_3(\xi)}{L_1(\xi)} (\mathbf{D} : \mathbf{nn}) \mathbf{M} \right]$$

$$-2D_r\mathbf{M} + D_r \left[\left(1 - \frac{L_1(\xi)}{\xi} \right) \mathbf{h} - \frac{L_2(\xi)}{L_1(\xi)} (\mathbf{h} \cdot \mathbf{n}) \mathbf{M} \right]. \quad (8)$$

Functions $L_i(x)$ are defined recursively by $L_{i+1}(x) = L_{i-1}(x) - (2i+1)L_i(x)/x$, with $L_0(x) = 1$ and $L_1(x)$ the Langevin function. The accuracy of the EFA has been discussed, e.g., in Refs. [17,18,19,20].

The defect (3) of this approximation can be calculated explicitly. Note, that $\int d^2u \Delta_{\mathbf{M}}$ as well as $\int d^2u \mathbf{u} \Delta_{\mathbf{M}}$ vanish identically by construction. Therefore, we estimate the accuracy of the EFA through information about the dynamics of the next higher order moment that is not included in the macroscopic description and consider the matrix $\Delta_{\mathbf{M}} = \int d^2u \mathbf{u} \mathbf{u} \Delta_{\mathbf{M}}$. As a suitable norm we use the matrix norm $\|\Delta\| = \sqrt{\sum_{\alpha\beta} (\Delta_{\alpha\beta})^2}$. The matrix $\Delta_{\mathbf{M}}$ can be represented by

$$\Delta_{\mathbf{M}} = d_1 \mathbf{1} + d_2 \mathbf{nn} + d_3 (\mathbf{hn} + \mathbf{nh}) + d_4 \mathbf{D} + d_5 (\mathbf{D} \cdot \mathbf{nn} + \mathbf{nn} \cdot \mathbf{D}), \quad (9)$$

where the coefficients d_i are defined in the Appendix A.

4 Numerical implementation

The microscopic dynamics (6) is integrated by Brownian dynamics simulations of the corresponding Itô stochastic differential equation

$$d\mathbf{U}_t = \mathbf{P}_t \cdot [(\boldsymbol{\Omega} \times \mathbf{U}_t + B\mathbf{D} \cdot \mathbf{U}_t + \mathbf{h}) dt + d\mathbf{W}_t] - \mathbf{U}_t \frac{dt}{\tau}. \quad (10)$$

The projector perpendicular to \mathbf{U}_t is denoted by $\mathbf{P}_t \equiv (\mathbf{1} - \mathbf{U}_t \mathbf{U}_t)$ and \mathbf{W}_t is a three-dimensional Wiener process [21]. Using Itô's formula, it is verified that Eq. (10) conserves the normalization of \mathbf{U}_t . Eq. (10) is integrated numerically by a weak first-order scheme that guarantees the normalization of the random unit vector \mathbf{U}_t [21]. An ensemble of 10^5 random vectors \mathbf{U}_t is used in the simulation in order to ensure accurate ensemble averages. A constant time step $\Delta t/\tau = 10^{-3}$ is used throughout.

The macroscopic equation (8) is integrated directly in terms of the macroscopic variables \mathbf{M} . The effective field ξ is calculated by $\xi = L_1^{-1}(M)$, where M denotes the norm of \mathbf{M} and $L_1^{-1}(x)$ denotes the inverse Langevin function. The latter is evaluated numerically by the Newton-Raphson Method. In order to treat microscopic and macroscopic dynamics approximately on the same footing, we used a first-order explicit Euler scheme with the same time step $\Delta t/\tau = 10^{-3}$ to integrate Eq. (8) numerically. More accurate schemes for the

macroscopic equation, such as Runge–Kutta methods, could be employed as well.

At every time step of the microscopic or macroscopic integration, the norm of the defect of invariance $\|\Delta\|$ is evaluated from Eq. (9). If in the course of the microscopic integration the inequality $\|\Delta\| < \epsilon$ is satisfied at time t , then the microscopic simulation is stopped and the macroscopic integration of Eq. (8) is started with the initial condition $\mathbf{M}(t)$ calculated from the microscopic ensemble average. On the other hand, if at time t during the integration of the macroscopic equation $\|\Delta\| > \epsilon$ is fulfilled, the microscopic simulation is started with initial condition $f(\mathbf{u}; t) = f_{\mathbf{M}(t)}(\mathbf{u})$. Here, we use the rejection method [22] in order to generate an ensemble of random unit vectors \mathbf{U}_t , which are distributed according to $f_{\mathbf{M}(t)}(\mathbf{u})$.

5 Results

The combined integration scheme described above has been implemented and run for a number of different values of magnetic field and velocity gradients. We limited ourselves to the case of plane shear flow. Previous investigations showed that the EFA provides a good approximation to the kinetic equation (6) for moderate values of axes ratios r [20]. We here choose a value of $r = 5$ in the sequel, where the accuracy of the EFA is not as good as for smaller values.

First, we consider the dynamics in the absence of any velocity gradients where a constant magnetic field h is applied during the time interval $t_i \leq t \leq t_f$. Comparison of the BD simulation results and the EFA for $h = 2$ and $h = 5$ with $t_i = \tau$, $t_f = 4\tau$ is shown in Fig. 2. From Fig. 2 we observe that the EFA provides a very good approximation for this case. Deviations of the EFA from the results of the BD simulation are shown in Fig. 3 together with the values of the norm of the defect of invariance. As can be seen from Fig. 3, the defect is very sensitive to deviations of the EFA from the BD results. Upon closer inspection one recognizes from Fig. 3 that the maxima of the defect precede the extrema of the deviations, reflecting the fact that the defect of invariance is sensitive to deviations in the time derivative. Thus, the defect signals the inaccuracy of the time derivative of the EFA and allows for a switch to the BD simulation before the values of the magnetization become inaccurate. The result of the combined integration scheme with $\epsilon = 0.2$ is shown in Fig. 4. Within the boxed regions, the norm of the defect of invariance $\|\Delta\| > \epsilon$ and the BD simulation is performed while otherwise the EFA is integrated. In the inset of Fig. 4, the result of the EFA, Fig. 2, is shown for comparison. Clearly, the combined integration improves the comparison of the EFA to the BD simulation.

Next, we consider the magnetization dynamics in the presence of flow. Starting with an isotropic initial distribution in the absence of magnetic fields and velocity gradients, a constant magnetic field h is applied during the interval $t_i \leq t \leq t_f$, while the magnetic field is absent outside this interval. In addition, a plane Couette flow with velocity field $\mathbf{v} = (2\dot{\gamma}y, 0, 0)$ with a constant shear rate $\dot{\gamma}$ is applied during the interval $t_1 \leq t \leq t_2$ while no shear is applied for $t < t_1$ and $t > t_2$. Fig. 5 shows the magnetization dynamics for $h = 5$, $\tau\dot{\gamma} = 2$, $t_i = \tau$, $t_f = 6\tau$, $t_1 = 3\tau$, and $t_2 = 8\tau$. One observes from Fig. 5 that the EFA predicts qualitatively correct behavior but fails to give accurate results as long as the shear flow is applied. Fig. 6 shows the deviation of the EFA from the BD simulation results together with the norm of the defect of invariance. Except for initial transient dynamics when the magnetic field is suddenly applied (see Fig. 3) the EFA is accurate in the absence of shear flow and $\|\Delta\|$ is small. During application of the shear flow, however, the predictions of the EFA are less accurate as is monitored by $\|\Delta\|$. In Fig. 7 we show the result of the combined integration scheme for the present situation where $\epsilon = 0.2$. The agreement between the combined scheme with the BD simulation is very good. Due to the low accuracy of the EFA, the macroscopic equation (8) is integrated only in the boxed regions while otherwise BD simulations are performed.

Finally, we consider the magnetization dynamics in a constant magnetic field h and a plane Couette flow $\mathbf{v} = (2\dot{\gamma}y, 0, 0)$ with oscillatory shear rate $\dot{\gamma} = \omega\gamma_0 \cos(\omega t)$. The magnetic field is oriented in the flow direction. Equilibrium initial conditions are chosen. Due to the flow, a nonequilibrium magnetization component M_y arises which oscillates with frequency ω , while the magnetization component in the magnetic field direction M_x oscillates with frequency 2ω . From Fig. 8 we observe that the predictions of the EFA are less reliable compared to the situation without flow. The deviation of both magnetization components are shown in Fig. 9 together with the defect of invariance. The deviation of the magnetization components of the macroscopic dynamics (EFA) from the microscopic dynamics (BD) are seen to oscillate as well. While the deviation of M_y oscillates around zero, the macroscopic dynamics always overpredicts the values of M_x in the present case. The oscillations in the deviation of M_x and M_y are reflected in the oscillations of $\|\Delta\|$. As before, the maxima of $\|\Delta\|$ occur before the maximum deviations of the magnetization are observed. Note that $\|\Delta\|$ always exceeds a certain value ϵ_0 , which signals the inaccuracy of the EFA in the present case. Fig. 10 shows the result of the combined integration scheme with $\epsilon = 0.2$ for the same conditions as in Fig. 8. In the boxed regions $\|\Delta\| < \epsilon$ and the macroscopic (EFA) dynamics is integrated while otherwise BD simulations are performed. The agreement between combined integration and BD simulation is very good. However, due to the limited accuracy of the EFA for this case only a limited fraction of the total integration time is performed with the EFA. Fig. 11 shows the same situation as in Fig. 8, but the shear flow was stopped at time $t = 6.5\tau$ while the magnetic field remained unchanged. Without the terms arising from the

velocity gradient, $\|\Delta\|$ drops below the threshold value ϵ and, within the combined scheme, the relaxational dynamics for $t > 6.5\tau$ is integrated by the EFA. Good agreement with the result of full BD simulation is found.

6 Conclusions

The present approach of combined microscopic and macroscopic simulation exploits the invariance of the microscopic relative to the macroscopic dynamics. It is applicable whenever a macroscopic description to an underlying microscopic dynamics is given. While previous studies considered the case of dilute polymer solutions [8,9], the combined integration scheme is illustrated here for the case of ferrofluid dynamics.

The microscopic dynamics is integrated only if the defect of invariance exceeds a certain threshold value ϵ . The full microscopic simulation is recovered for $\epsilon = 0$ while $\epsilon \rightarrow \infty$ corresponds to the macroscopic dynamics. Thus, the combined integration improves the accuracy of the macroscopic description, where the improvement depends on the choice of ϵ . At the same time, the combined integration saves CPU time since the macroscopic simulation is employed whenever possible. The amount of CPU time that can be saved by the combined integration scheme for a given value of ϵ depends on the quality of the macroscopic description for the corresponding situation. For the conditions of Fig. 8, a sample study of the relative error R_x of the magnetization M_x as a function of elapsed CPU time is shown in Fig. 12. The relative error with respect to the result of the BD simulation is defined as $R_x^2 = \frac{1}{N_t} \sum_j^{N_t} [(M_x(t_j) - M_x^{\text{BD}}(t_j))/M_x^{\text{BD}}(t_j)]^2$, where N_t denotes the total number of integration time steps. For a better comparison, all data shown in Fig. 12 are obtained with the same PC with a P4 processor. From Fig. 12 we observe that the relative error decreases with decreasing ϵ while the time the microscopic simulation is integrated in the combined scheme increases and thus the required CPU time increases. Overall, we observe that the relative error decreases almost linearly with elapsed CPU time. Note, that $R_x = 0$ does not correspond to the exact result but to the BD simulation.

Acknowledgment

Valuable discussions with A. N. Gorban, H.C. Öttinger, and S. Hess are gratefully acknowledged. This work was supported in part by DFG priority program SPP 1104 'Colloidal Magnetic Fluids' under grant no. HE1100/6-2.

A Coefficients of defect of invariance

The coefficients d_i in Eq. (9) contain contributions from Brownian motion, the magnetic field and the symmetric velocity gradient. In particular,

$$d_1 = 2(L_2(\xi) + c(\xi)) \left(1 - \frac{\mathbf{n} \cdot \mathbf{h}}{\xi}\right) - B \left(2\frac{L_3(\xi)}{\xi} + \frac{3L_2(\xi)}{\xi L_1(\xi)}c(\xi)\right) (\mathbf{D} : \mathbf{nn}) \quad (\text{A.1})$$

$$\begin{aligned} d_2 = & -6(L_2(\xi) + c(\xi)) \left(1 - \frac{\mathbf{n} \cdot \mathbf{h}}{\xi}\right) + 2 \left(L_2(\xi) \left[\frac{1}{L_1(\xi)} - \frac{4}{\xi}\right] - L_3(\xi)\right) \mathbf{n} \cdot \mathbf{h} \\ & + \frac{B}{\xi} \left(14L_3(\xi) - 4\frac{L_2^2(\xi)}{L_1(\xi)} + 9\frac{L_2(\xi)}{L_1(\xi)}\right) \mathbf{D} : \mathbf{nn} \end{aligned} \quad (\text{A.2})$$

$$d_3 = L_1(\xi) - L_2(\xi) \left(\frac{1}{L_1(\xi)} - \frac{1}{\xi}\right) \quad (\text{A.3})$$

$$d_4 = \frac{2B}{\xi} \left(L_1(\xi) - \frac{2L_2(\xi)}{\xi}\right) \quad (\text{A.4})$$

$$d_5 = \frac{2B}{\xi} \left(\frac{L_2^2(\xi)}{L_1(\xi)} - 2L_3(\xi)\right), \quad (\text{A.5})$$

where

$$c(\xi) = \frac{L_1(\xi)}{\xi L_1'(\xi)} [L_2(\xi) - L_1(\xi)^2] \quad (\text{A.6})$$

and the total derivative of the Langevin function can be expressed by

$$L_1'(\xi) \equiv \frac{dL_1(\xi)}{d\xi} = 1 - \frac{2L_1(\xi)}{\xi} - L_1^2(\xi). \quad (\text{A.7})$$

References

- [1] P. Ilg, I. V. Karlin, H. C. Öttinger, Canonical distribution functions in polymer dynamics: I. Dilute solutions of flexible polymers, *Physica A* 315 (2002) 367-385.
- [2] P. Ilg, M. Kröger, I. V. Karlin, H. C. Öttinger, Canonical distribution functions in polymer dynamics: II. liquid-crystalline polymers, *Physica A* 319C (2003) 134-150.
- [3] A. N. Gorban, P. A. Gorban, I. V. Karlin, Legendre integrators, post-processing and quasiequilibrium, *J. Non-Newton. Fluid Mech.*, this issue.
- [4] M. Laso and H. C. Öttinger, Calculation of viscoelastic flow using molecular models - the CONNFESSIT approach, *J. Non-Newton. Fluid Mech.* 47 (1993) 1-20.
- [5] R. M. Jendrejack, J. J. de Pablo, M. D. Graham, A method for multiscale simulation of flowing complex fluids, *J. Non-Newton. Fluid Mech.* 108 (2002) 123-142.
- [6] C. I. Siettos, M. D. Graham, I. G. Kevrekidis, Coarse Brownian dynamics for nematic liquid crystals: Bifurcation, projective integration, and control via stochastic simulation, *J. Chem. Phys.* 118 (2003) 10149-10156.
- [7] R. B. Bird, J. M. Wiest, Constitutive equations for polymeric liquids, *Ann. Rev. Fluid Mech.* 27 (1995) 169-193.
- [8] A. N. Gorban, I. V. Karlin, P. Ilg, H. C. Öttinger, Corrections and enhancements of quasi-equilibrium states, *J. Non-Newton. Fluid Mech.* 96 (2001) 203-219.
- [9] I. V. Karlin, P. Ilg, H. C. Öttinger, Invariance principle to decide between micro and macro computations in *Recent Developments in Mathematical and Experimental Physics, Volume C: Hydrodynamics and Dynamical Systems*. p. 43-50, F. Uribe (Ed.), Kluwer, Dordrecht, 2002.
- [10] A. N. Gorban and I. V. Karlin, Thermodynamic parameterization, *Physica A* 190 (1992) 393-404.
- [11] A. N. Gorban, I. V. Karlin, A. Y. Zinovyev, Constructive methods of invariant manifolds for kinetic problems, preprint 2003, available at <http://www.ihes.fr/PREPRINTS/M03/Resu/resu-M03-50.html>.
- [12] E. Blums, A. Cebers, M. M. Maiorov, *Magnetic Fluids*. de Gruyter, Berlin, 1997.
- [13] M. Kröger, P. Ilg, S. Hess, Magnetoviscous model fluids, *J. Phys. Condens. Matter* 15 (2003) S1401-S1423.
- [14] M. A. Martsenyuk, Viscosity of a suspension of ellipsoidal ferromagnetic particles in a magnetic field, *J. Appl. Mech. Tech. Phys.* 14 (1973) 564-566.

- [15] A. Cebers, Simulation of the magnetic rheology of a dilute suspension of ellipsoidal particles in a numerical experiment, *Magnetohydrodynamics* 20 (1984) 349-354.
- [16] S. Hess, Fokker-Planck-Equation approach to flow alignment in liquid crystals *Z. Naturforsch.* 31a (1976) 1034.
- [17] M. A. Martsenyuk, Yu. L. Raikher, M. I. Shliomis, On the kinetics of magnetization of suspension of ferromagnetic particles, *Sov. Phys. JETP* 38 (1974) 413-416.
- [18] P. Ilg, M. Kröger, S. Hess, Orientational Order Parameters and Magnetoviscosity of Dilute Ferrofluids, *J. Chem. Phys.* 116 (2001) 9078-9088.
- [19] P. Ilg and M. Kröger, Magnetization dynamics, rheology, and an effective description of ferromagnetic units in dilute suspension, *Phys. Rev. E* 66 (2002) 021501.
- [20] P. Ilg, M. Kröger, S. Hess, A. Yu. Zubarev, Dynamics of colloidal suspensions of ferromagnetic particles in plane Couette flow: comparison of approximate solutions with Brownian dynamics simulations, *Phys. Rev. E* 67 (2003) 061401.
- [21] H. C. Öttinger, *Stochastic Processes in Polymeric Fluids*. Springer, Berlin, 1996.
- [22] W. H. Press, S. A. Teukolsky, W. T. Vetterling, B. P. Flannery, *Numerical Recipes in Fortran*. Cambridge University Press, 2nd ed. 1992.

Figure captions:

Fig. 1 Sketch of the combined integration scheme. The macroscopic dynamics is integrated whenever the norm of the defect of invariance $\|\Delta\|$ is smaller than some fixed threshold value ϵ . Otherwise, the microscopic dynamics is integrated.

Fig. 2 Magnetization dynamics as a function of reduced time t/τ in the absence of velocity gradients. A constant magnetic field h was applied during the time interval $1 \leq t/\tau \leq 4$, while the magnetic field was switched off outside this interval. Circles and squares are the results of the BD simulation for $h = 5$ and $h = 2$, respectively, while solid and dashed line are the corresponding predictions of the EFA. The inset shows the comparison for $h = 5$ on a finer scale.

Fig. 3 Deviation of normalized magnetization M_x/M_{sat} calculated from BD simulation and the EFA for $h = 5$ (circles) and $h = 2$ (squares) for the same conditions as in Fig. 2. Solid and dashed lines are the defect of invariance as calculated from the matrix norm of Eq. (9) for $h = 5$ and $h = 2$, respectively. For better visibility, the matrix norm was multiplied by a factor 0.1.

Fig. 4 Magnetization dynamics as a function of reduced time t/τ for the same condition as in Fig. 2. Circles and squares are the result of the BD simulation for $h = 5$ and $h = 2$, respectively, while solid and dashed lines are the results of the combined integration scheme with $\epsilon = 0.2$ for $h = 5$ and $h = 2$, respectively. Within the boxed regions (indicated by the shading in the upper part), $\|\Delta\| > \epsilon$ and the BD simulation is performed, otherwise the EFA is integrated. The inset shows the comparison for $h = 5$ on a finer scale, where the dashed-dotted line is the result of the EFA.

Fig. 5 Magnetization dynamics as a function of reduced time t/τ in a constant magnetic field $h = 5$ for $1 \leq t/\tau \leq 6$ and steady shear flow with shear rate $\tau\dot{\gamma} = 2$ for $3 \leq t/\tau \leq 8$, where the magnetic field is oriented in the gradient direction. No magnetic field and no shear flow is applied outside the mentioned time intervals. Circles and squares represent the results of the BD simulation for M_x/M_{sat} and M_y/M_{sat} , respectively, while solid and dashed lines are the corresponding result of the EFA.

Fig. 6 Deviation of normalized magnetization M_x/M_{sat} (circles) and M_y/M_{sat} (squares) calculated from BD simulation and the EFA for the same conditions as in Fig. 5. The solid line is the defect of invariance as calculated from the matrix norm of Eq. (9). For better visibility, the matrix norm was multiplied by a factor 0.1.

Fig. 7 Magnetization dynamics as a function of reduced time t/τ for the same conditions as in Fig. 5. Circles and squares represent the result of full BD simulation, the dashed-dotted line corresponds to the EFA and full lines are the result of the combined integration scheme, where the EFA is integrated within the boxed regions while otherwise BD simulations are performed.

Fig. 8 Magnetization dynamics as a function of reduced time t/τ for inception of oscillatory shear flow with frequency $\tau\omega = 2$ and amplitude

$\gamma_0 = 0.5$. The magnetic field is oriented in flow direction with $h = 2$. Circles and squares represent the results of the BD simulation for M_x/M_{sat} and M_y/M_{sat} , respectively, while solid and dashed lines are the corresponding result of the EFA.

Fig. 9 Deviation of normalized magnetization M_x/M_{sat} (circles) and M_y/M_{sat} (squares) calculated by BD simulation and from EFA as functions of time t/τ . Also shown is the norm of defect of invariance $\|\Delta\|$ (solid line), which is multiplied by a factor 0.1 for better visibility. The same flow conditions as in Fig. 8 are considered.

Fig. 10 Magnetization dynamics as a function of reduced time t/τ for the same conditions as in Fig. 8. Symbols are the result of the BD simulation. Solid and dashed lines correspond to the combined integration, where the EFA is integrated within the boxed regions (indicated by the shading in the upper part) and the BD simulation is preformed outside.

Fig. 11 Magnetization dynamics as a function of reduced time t/τ for the same conditions as in Fig. 8, but where the shear flow was stopped at time $t = 6.5\tau$. Symbols are the result of the BD simulation. Solid and dashed lines correspond to the combined integration, where the EFA is integrated within the boxed regions (indicated by the shading in the upper part) and the BD simulation is preformed outside. Dashed-dotted lines are the result of the EFA.

Fig. 12 Relative error R_x defined in the text as a function of CPU time in seconds on a logarithmic scale. The same conditions as in Fig. 8 are considered. The number above the filled symbols are the corresponding values of ϵ . Solid lines are guides to the eye. Different values of ϵ decreasing from $\epsilon = 1$ (EFA) to $\epsilon = 0$ (BD simulation) have been chosen in the combined integration scheme in order to obtain increasingly more accurate results for M_x .

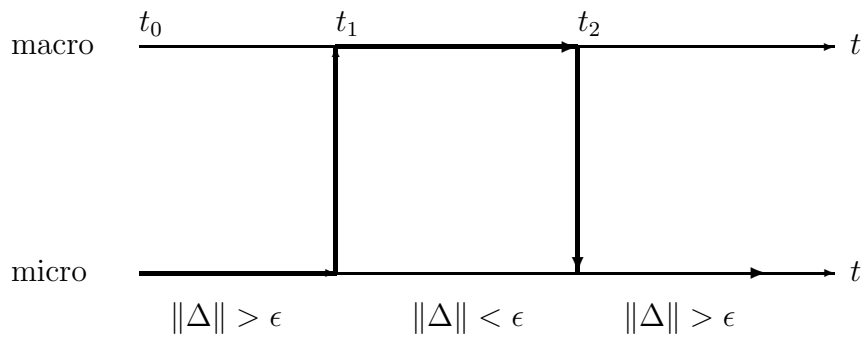


Fig. 1.

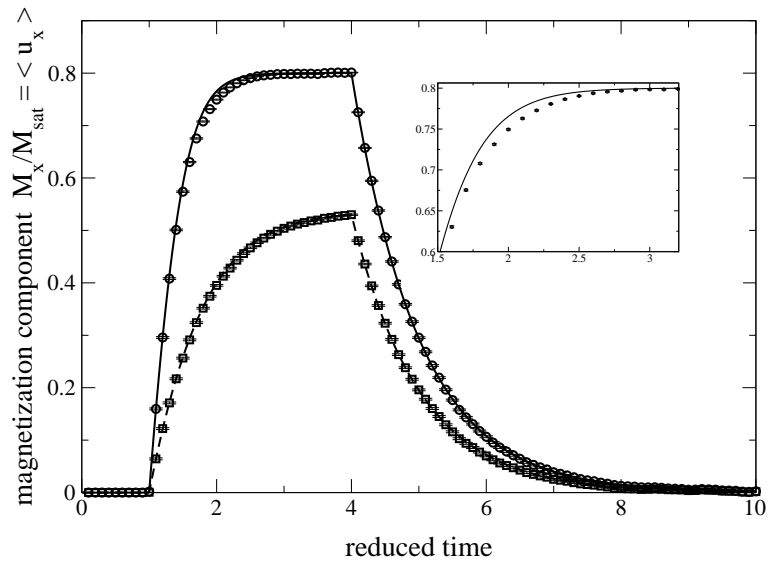


Fig. 2.

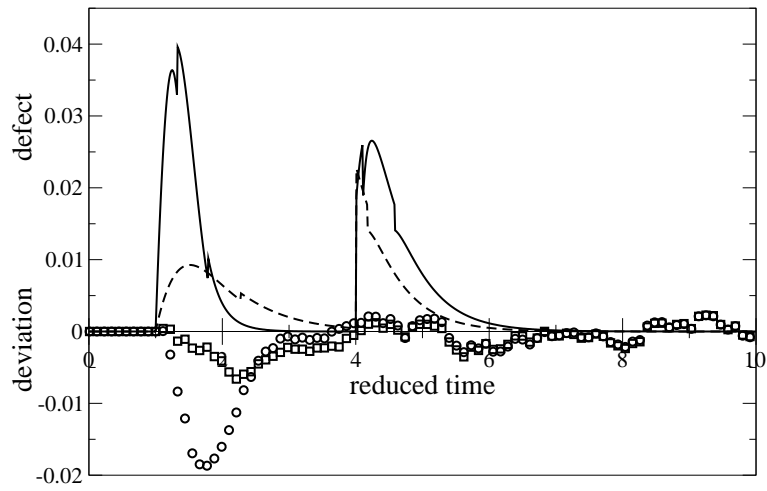


Fig. 3.

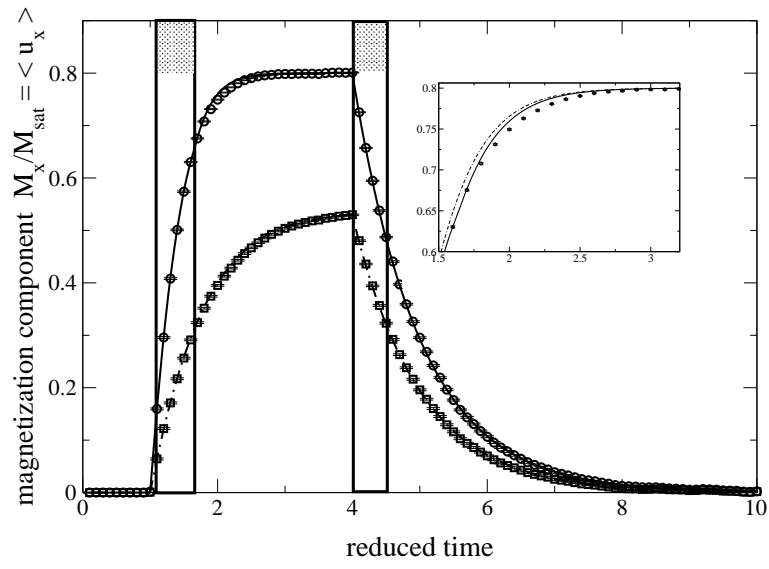


Fig. 4.

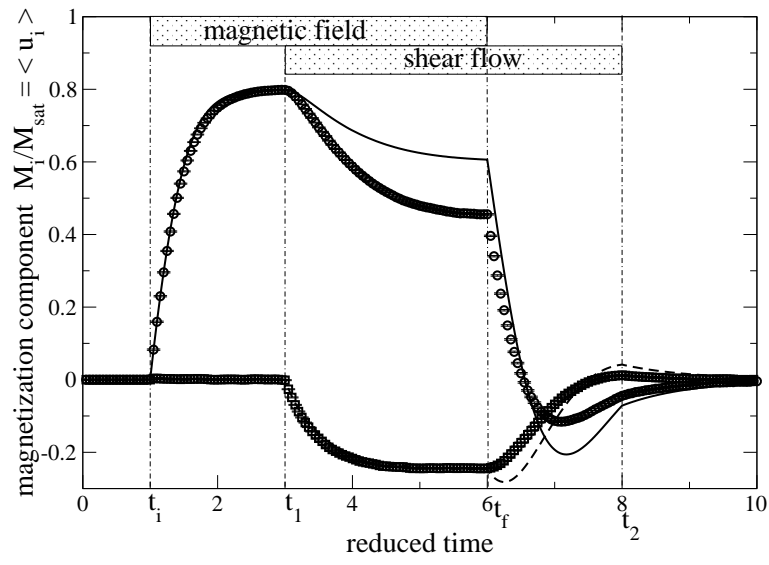


Fig. 5.

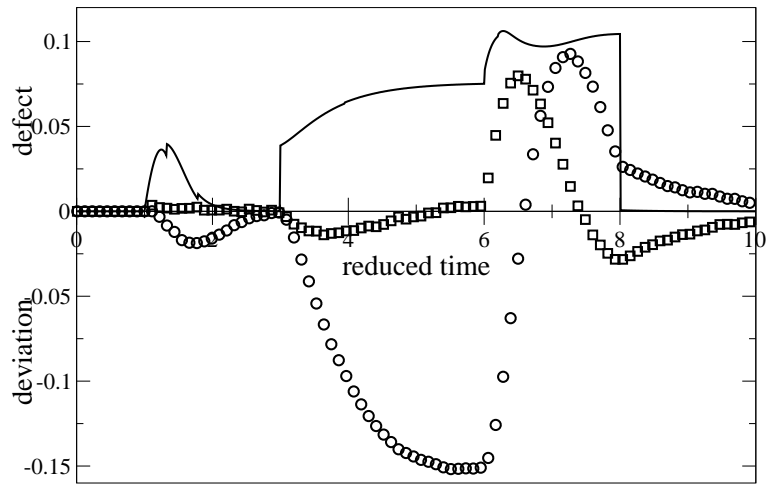


Fig. 6.

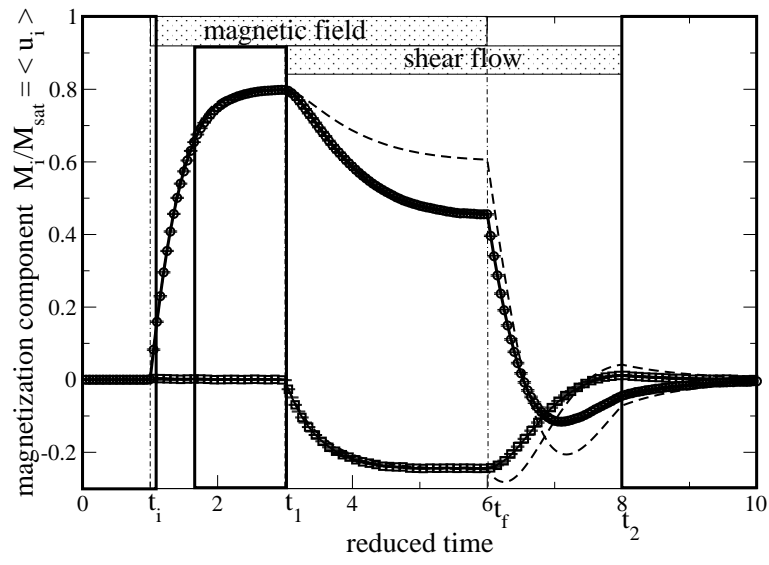


Fig. 7.

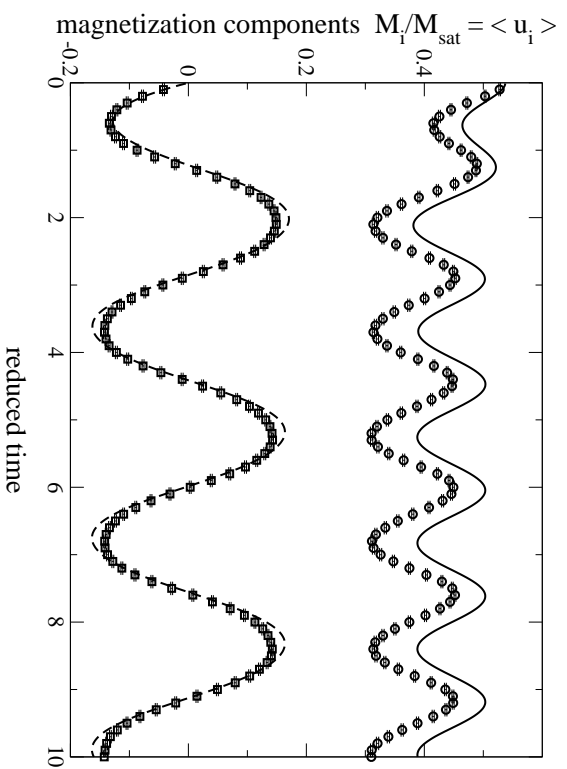


Fig. 8.

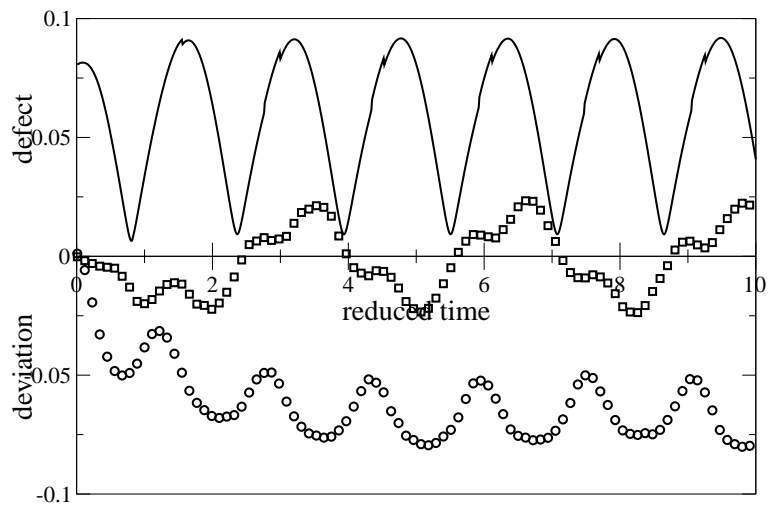


Fig. 9.

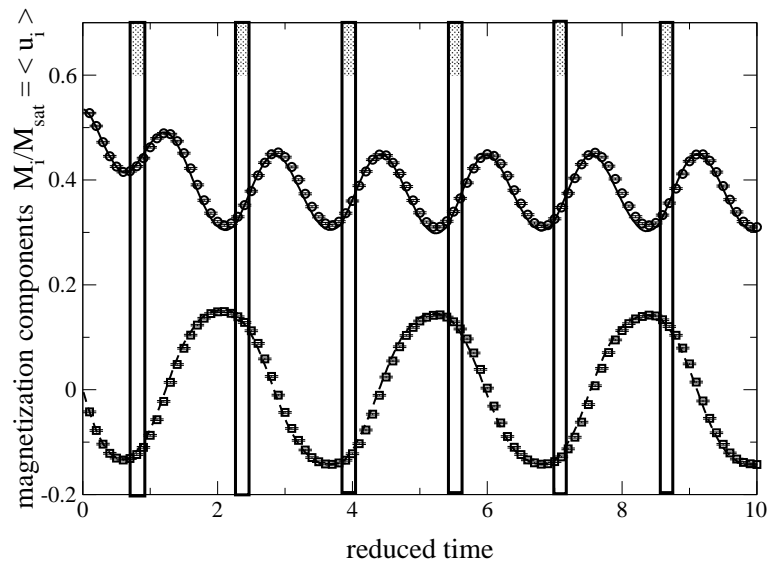


Fig. 10.

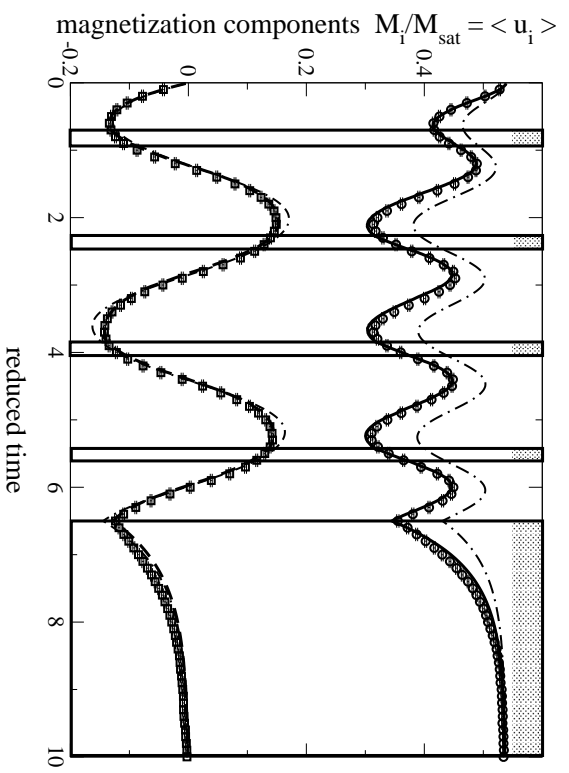


Fig. 11.

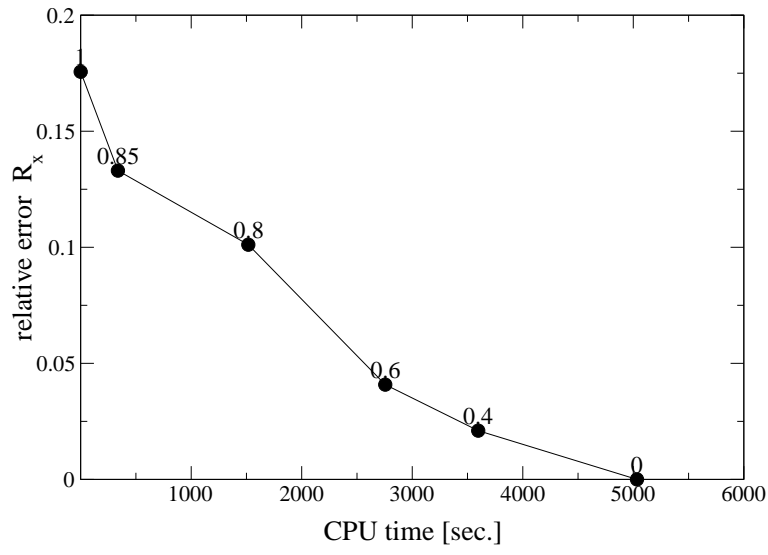


Fig. 12.